applied sciences

MDPI

Article

Stability Maintenance of Gravity Comparison Sites (2017–2024): Environmental Factors and Data Processing Strategies

Lishuang Mou [1,2], Dong Wang [1,2], Jinyang Feng [1,2], Qiyu Wang [1,2], Jiamin Yao [1,2], Huijuan Ma [3], Xiaodong Chen [4,5], Chunjian Li [1,2,*] and Miaomiao Zhang [4,5,*]

1 National Institute of Metrology (NIM), Beijing 100029, China; mouls@nim.ac.cn (L.M.); wangd@nim.ac.cn (D.W.); fengjy@nim.ac.cn (J.F.); wangqiyu@nim.ac.cn (Q.W.); yaojm@nim.ac.cn (J.Y.)
2 Key Laboratory of Time Frequency and Gravity Primary Standard, State Administration for Market Regulation, Beijing 100029, China
3 National Key Laboratory of Metrology and Calibration, Beijing Changcheng Institute of Metrology & Measurement, Beijing 100095, China; mahj005@avic.com
4 State Key Laboratory of Precision Geodesy, Innovation Academy for Precision Measurement Science and Technology, Chinese Academy of Sciences, Wuhan 430077, China; chenxd@apm.ac.cn
5 Wuhan Geodesy National Observation and Research Station, Innovation Academy for Precision Measurement Science and Technology, Chinese Academy of Sciences, Wuhan 430077, China
* Correspondence: lichj@nim.ac.cn (C.L.); zhangmm@apm.ac.cn (M.Z.)

Abstract

To ensure the sustained stability of absolute gravity benchmark points from 2017 to 2024, observational records from superconducting gravimeters (SGs) and absolute gravimeters were comprehensively examined in this work, and the environmental effects on gravitational acceleration were quantitatively assessed. The annual fluctuation of the SG (iGrav-012k) scale factor reached 0.268 μGal/V, with a weighted average of (–92.8702 ± 0.0265) μGal/V (relative precision of 0.3‰), providing a precise scale factor for long-term SG monitoring. By removing step discontinuities in the SG data using FG5-X249 absolute gravimeter measurements, the residual fitting error decreased to 6.3 μGal. In addition, the SG drift was estimated as 1.0 μGal/year through international comparison datasets and FG5 measurements, substantially improving the consistency of the time series. Further investigation showed that the SG residuals exhibited clear seasonal oscillations, which were mainly attributed to local hydrological processes and ground deformation near the benchmark sites. By integrating groundwater level and deformation monitoring data and applying a neural network model to separate hydrological load components, the peak-to-peak residual amplitude was reduced from 13 μGal to 3.5 μGal. Quantitative analysis indicated that hydrological effects contributed about 9.5 μGal to the seasonal variation, whereas surface deformation had only a minor impact (<2 μGal). The findings confirm that careful data correction and isolation of environmental effects are effective for maintaining the long-term stability of gravity benchmarks. The developed workflow provides a reproducible framework for high-precision gravity site maintenance and supports future dynamic monitoring of regional environmental load responses.

Keywords: superconducting gravimeter; seasonal gravity variation; absolute gravity benchmark points

Check for updates

Academic Editor: Tiago Filipe da Silva Miranda

Received: 6 May 2026
Revised: 2 June 2026
Accepted: 3 June 2026
Published: 5 June 2026

Copyright: © 2026 by the authors. Licensee MDPI, Basel, Switzerland. This article is an open access article distributed under the terms and conditions of the Creative Commons Attribution (CC BY) license.

1. Introduction

Accurate measurement of gravitational acceleration is an essential requirement in Earth science, resource exploration, and space research [1]. The intercomparison of absolute

gravimeters and the preservation of gravity comparison points are necessary for maintaining traceability and reliability in gravity metrology. In 2017, the 10th International Absolute Gravity Comparison, organized by the Chinese Institute of Metrology, reinforced the global gravity standard and supported the temporal stability of reference sites [2,3]. However, during continuous superconducting gravimeter observations, maintaining data completeness and separating environmental disturbances have become important challenges affecting long-term reliability.

As the superconducting gravimeter (SG) is a relative gravimeter operating on the principle of superconducting magnetic levitation, the precision of its scale factor and drift directly influences the reliability of continuous observation data. The procedure for determining the scale factor is relatively mature and usually includes simultaneous co-located observations with an absolute gravimeter (FG5) [4–6]. Many researchers have examined optimal strategies for obtaining high-precision scale factors, including the length of simultaneous observations [7] and the use of individual drop values rather than pre-averaged set values (each set consisting of 100 drops) in the fitting process [8,9]. Because the superconducting gravimeter at the reference site is employed for continuous observations over several years, not only a precise scale factor but also its temporal change should be monitored. The most widely used approach for estimating SG drift is still periodic co-located observations with an FG5. For continuous observation records covering less than ten years, a linear drift model is considered appropriate, whereas for records exceeding ten years, an exponential function is more suitable [10]. The WULG laboratory in Luxembourg investigated the drift behavior of two superconducting gravimeters and demonstrated that power interruptions lasting less than three days do not alter the long-term linear drift but do induce steps in the gravity record. Since the superconducting gravimeter at the reference site also experiences power interruptions that cause discontinuities in the continuous gravity record, accurate treatment of these steps is required in addition to precise drift estimation. The commonly used software Tsoft (V2.2.11) can be employed to correct such steps; however, this approach may introduce significant errors. In contrast to the traditional manual Tsoft method, which relies on visual judgment and lacks quantitative repeatability, the segment-wise linear fitting method proposed in this study can quantitatively determine step magnitudes with high repeatability. This is particularly important for gravity benchmark sites responsible for quantity transmission and metrological traceability. Therefore, Section 5 of this paper presents a method for quantitatively determining both SG drift and step corrections.

The continuous superconducting gravity observations contain environmental gravity signals that must be removed to reveal the long-term stability of the reference benchmark. Gravity variations induced by atmospheric pressure, polar motion, and solid Earth tides can be removed through well-established models. Hydrological effects can be simulated using MERRA-2 reanalysis data, and the modeled hydrological gravity contribution can then be subtracted from the superconducting gravimeter observations. However, previous studies have shown that residual noise in the 1- to 10-day period band persists after such subtraction, likely because of the insufficient spatial resolution of MERRA-2 [11]. The gravimeter records an integrated signal in which contributions from local, regional, and larger scales cannot be readily separated, making it difficult to directly compare conventional hydrological models with superconducting gravimeter observations [12]. To address the spatial resolution limitation of global reanalysis products (MERRA-2, 50 km), this study employs a neural network combined with correlation analysis using local in situ water-level measurements to effectively capture local-scale hydrological signals and remove the groundwater contribution from gravity residuals. In addition, gravity changes caused by ground deformation are evaluated using satellite-based ground deformation observations.

A comparative analysis shows that groundwater-level variation is the dominant factor driving seasonal gravity fluctuations.

A preliminary version of this work has previously been deposited as a preprint [13]. This study proposes the following integrated framework.

The main contributions of this study are as follows:

(1) Long-term observational evidence: Based on seven years (2017–2024) of superconducting gravimeter (iGrav-012k) and absolute gravimeter (FG5-X249) data, we characterize seasonal gravity variations at absolute gravity benchmark sites and provide precise calibration parameters for long-term SG monitoring.
(2) Quantitative separation of environmental effects: Using a neural network model, we separate the hydrological contribution from surface deformation effects (<2 μGal), demonstrating that hydrological processes dominate the seasonal gravity signal.
(3) Reproducible data processing workflow: Although previous studies have separately addressed SG calibration, drift estimation, hydrological effects, and deformation assessment, an integrated workflow that systematically combines these aspects specifically for gravity benchmark stability maintenance remains limited. We present a step-by-step workflow for maintaining the long-term stability of absolute gravity benchmark points, including SG drift estimation, step discontinuity removal, and hydrological load correction.

2. Data and Instruments

A superconducting gravimeter (SG, iGrav-012k, GWR Instruments, Suite D, San Diego, CA, USA) and an FG5-X249 absolute gravimeter (Micro-g LaCoste, Lafayette, CO, USA) were used in this study. The SG operated continuously from 2017 to 2024 at a sampling rate of 1 Hz, while the FG5 conducted periodic co-located measurements, collecting 100 drops per hour, with each campaign lasting 8–12 h.

Groundwater-level data were provided by the China Institute of Geo-Environment Monitoring and were recorded monthly at an observation well located approximately 7 km from the SG site. Surface deformation data for 2023–2024 were obtained from the Chinese Academy of Surveying and Mapping (CASM) via the National Surface Deformation Map Service Platform (https://deformation.casm.ac.cn) (accessed on 25 October 2025). The data were generated from 35 scenes of Sentinel-1 SAR images using the MCTSB InSAR technique, with a spatial resolution of 0 m and an accuracy of 4.5 mm/year.

3. Preprocessing

The SG recorded continuously at a sampling rate of 1 Hz. Preprocessing of the SG data was performed using Tsoft software. A low-pass filter with a cutoff frequency of 0.0041667 Hz (corresponding to a period of 240 s) and a window length of 480 was applied, followed by downsampling to 1 min intervals. Gaps in the data were filled using linear interpolation in Tsoft. Solid Earth tides were corrected using Tsoft with tidal factors from the 2017 international comparison. Polar motion and atmospheric pressure corrections followed the same method as the 2017 comparison, using an atmospheric admittance of –0.3 μGal/mBar and polar motion data from IERS.

The FG5 collected 100 drops per hour. For the FG5 absolute gravimeter, no additional preprocessing was required. For groundwater-level data, monthly records were interpolated to match the SG time series. For surface deformation data, the CASM products were used directly without additional processing.

4. Superconducting Gravimeter's Scale Factor

The superconducting gravimeter, as a highly sensitive relative gravimeter, outputs voltage signals that must be converted into gravitational acceleration through a scale factor. The scale factor of a superconducting gravimeter is a critical parameter that converts the instrument output voltage (or count) into physically meaningful gravity variations, $\Delta g = K \cdot \Delta V$, where K is the scale factor (μGal/V or nm/s^2/V). As a relative instrument, the SG does not provide absolute gravity values; therefore, precise calibration is essential to ensure the long-term stability of the gravity record, reliably estimate instrumental drift, and separate environmental signals from true gravity changes. Any error in the scale factor propagates directly into the calibrated gravity series, potentially biasing the interpretation of both secular trends and transient signals. Four principal methods are typically used to determine this scale factor [12]:

(1) Long-term tidal observations [14]

Continuous tidal monitoring was performed for 2–3 years, and standard tidal amplitudes were used to calibrate the superconducting gravimeter.

(2) Calibration platforms [15]

Precision calibration platforms are employed to define the conversion coefficient between voltage and gravity.

(3) Mass-shift calibration [16]

Calibration was performed using a large movable mass (e.g., a "mass sled" or controlled displacement system).

(4) Co-located measurements with an absolute gravimeter FG5 [4] or a high-precision atom gravimeter [17,18]. Simultaneous observations were carried out with an absolute gravimeter at the same site.

In addition to the methods mentioned above, the scale factor of one superconducting gravimeter can be transferred to another superconducting gravimeter using the tidal analysis method. Among these methods, method (4) is the most widely adopted worldwide. Since the annual drift rate of a superconducting gravimeter is very small (it is currently less than 1 μGal), its influence is neglected when the scale factor is calculated. Hinderer (1991) [4] conducted 24 h continuous simultaneous measurements using a superconducting gravimeter and an FG5 absolute gravimeter, achieving a calibration precision of 0.72%. Y. Tamura attained 0.2% precision from four days of observations co-located with FG5-109 [19]. In China, Chen Xiaodong obtained 0.2% precision through five days of continuous observation using FG5-112 and a superconducting gravimeter [20]. In this research, the superconducting gravimeter was calibrated following the same approach. Data from the FG5 and the superconducting gravimeter were fitted using least-squares regression [7,21], as expressed by the following equation:

$$y_i = a + bx_i \quad (1)$$

In this expression, y_i represents the absolute gravimeter readings (μGal), and x_i corresponds to the superconducting gravimeter readings (V). The slope b denotes the scale factor (μGal/V), and a is the intercept (μGal). Measurements are typically conducted during spring tides, and neither gravimeter requires correction for barometric pressure or polar motion.

The calibration outcomes of the superconducting gravimeter at the Institute of Metrology, China, between 2017 and 2024 are summarized in Table 1 and illustrated in Figure 1. Detailed observation dates and durations for each calibration are given in Table 1.

Table 1. Scale factor table.

Start Time	Total Observation Duration/h	Data Number	Scale Factor and Precision/μGal/V
2017/11/01	80	8000	−92.7554 ± 0.0497
2018/05/15	73	7300	−92.8526 ± 0.0687
2019/01/04	60	6000	−92.9001 ± 0.1072
2020/08/03	64	6400	−92.8702 ± 0.0887
2021/06/09	25	2500	−92.8442 ± 0.1559
2022/12/07	72	7200	−92.9170 ± 0.1301
2023/12/26	72	7200	−92.7970 ± 0.0727
2024/11/01	60	6000	−93.0650 ± 0.0571

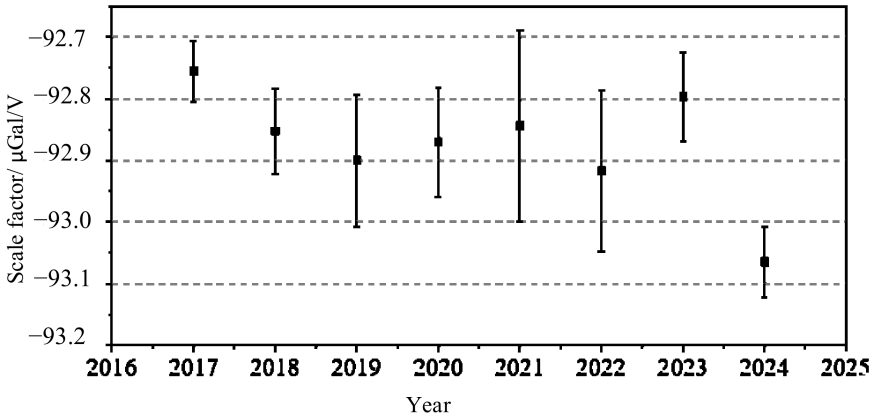

Figure 1. Scale factors.

Calibration is typically conducted during spring tides, with about 100 datasets collected per hour [4,22]. The calibration duration ranges from a minimum of 25 h to a maximum of 80 h. When the total number of drops exceeds 5000, both the calibration value and its precision become stable [23]. With the exception of the 2021 calibration, which involved a smaller data volume, all other calibration sessions recorded more than 5000 drops. The scale factor varied between –92.7 μGal/V and –93.1 μGal/V, with a maximum annual fluctuation of 0.268 μGal/V and a minimum of 0.026 μGal/V. Overall, the scale factor remained stable, indicating that no external interference occurred during the induction of the superconducting sphere within the magnetic fields of the upper and lower coils. The main reasons for the variation in the scale factor are as follows:

(1) Although the superconducting gravimeter and the absolute gravimeter were tested simultaneously in the same room, they were placed on two adjacent foundations, with slightly different annual gravity gradient changes.
(2) Some components of the superconducting gravimeter itself underwent slight changes over time.
(3) The FG5 measurement data had an uncertainty of 2 μGal, and the optical path alignment varied slightly across measurements.

The distribution of the scale factor and its standard deviation are shown in Figure 2. In 2024, construction activities within the campus affected gravity observations, resulting in a notable deviation. The weighted average of the scale factors from 2017 to 2024 is (–92.8702 ± 0.0265) μGal/V according to Formula 2 and Formula 3, corresponding to a

relative precision of 0.3‰. Subsequent SG data processing employed this weighted average scale factor.

$$\bar{b} = \frac{\sum_{i=1}^{n} \frac{b_i}{u_i}}{\sum_{i=1}^{n} \frac{1}{u_i^2}} \quad (2)$$

$$u\left(\bar{b}\right) = \frac{1}{\sqrt{\sum_{i=1}^{n} \frac{1}{u_i^2}}} \quad (3)$$

In this formula, b_i represents the calculated scale factor for each year, u_i denotes the corresponding precision, $\bar{b}$ is the weighted mean of the scale factor, n represents the number of calibrations, n = 8, and $u\left(\bar{b}\right)$ is the uncertainty of the weighted mean of the scale factor.

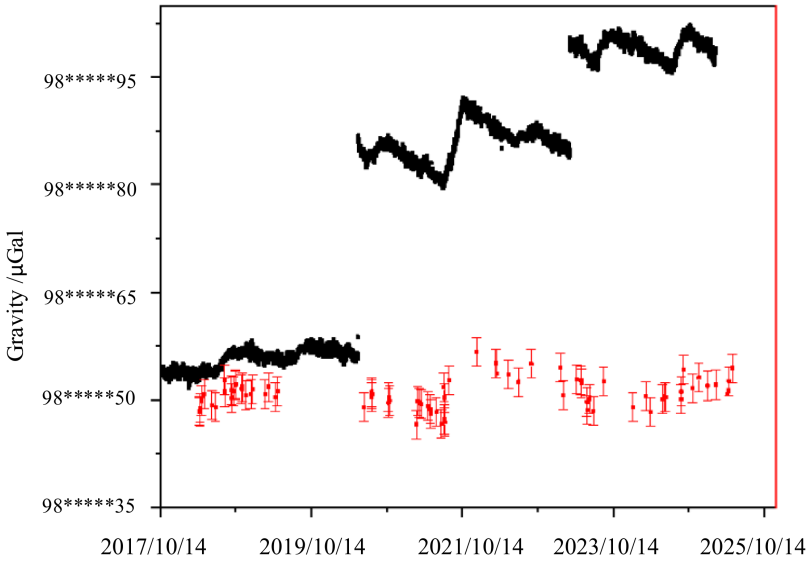

Figure 2. Gravity at the comparison sites (Red curve: FG5 absolute gravimeter measurements (±2 μGal). Black curve: combination of the 2017 comparison KCRV value and continuous SG observations. Both curves are corrected for solid Earth tides, polar motion, and atmospheric pressure, asterisks indicate parts of the gravity data that are not disclosed due to confidentiality restrictions).

5. Steps and Drift of the SG

5.1. Correction of the Steps

During the replacement of the cold head of the superconducting gravimeter in 2020 and 2023, the extended maintenance time led to helium depletion, resulting in step discontinuities in the SG observation data. To obtain continuous gravity observations, these steps required correction. After calibration, the FG5 and SG instruments were co-located for measurement, and corrections for solid Earth tides and polar motion were applied. The results are shown in Figure 2, where the black solid line denotes the SG observations linked to the 2017 international comparison point (KCRV value), and the red points represent the FG5 results with a 2 μGal uncertainty; SG precision is 0.1 μGal. Both datasets were corrected for solid Earth tides and polar motion. Because the KCRV represents absolute gravitational acceleration, the result linked with the superconducting gravimeter observations also represents absolute gravitational acceleration. For ease of comparison with the periodic FG5 measurements, the observation data from both instruments are plotted on the same vertical axis (the left-hand axis).

To maintain continuous gravity records at the comparison site, the step offsets in the SG data were modeled as follows:

$$g_1 - g_A = k \cdot t_1 + c_1 \quad (4)$$

$$g_2 - g_A = k \cdot t_2 + c_2 \quad (5)$$

$$g_3 - g_A = k \cdot t_3 + c_3 \quad (6)$$

Here, g_1, g_2, and g_3 are the three SG data segments; g_A denotes the corresponding FG5 observations; c_1–c_3 are the intercepts; and k is the SG drift. The difference (c_2–c_1) represents the first step magnitude, and (c_3–c_2) represents the second step.

Applying least-squares regression yielded c_1 = 5.4 μGal, k = 0.69 μGal/year, c_2 = 36.6 μGal, and c_3 = 51.8 μGal. Therefore, the 2020 step amplitude was 31.2 μGal, and the 2023 step was 15.2 μGal, with a residual variance of 6.3 μGal. Owing to personnel changes and imperfect beam waist corrections during long-term FG5 measurements, the derived drift may contain bias. Therefore, a refined drift model is introduced later. By integrating the step and drift corrections into the continuous SG data, the resulting absolute gravity time series (Figure 3) was obtained.

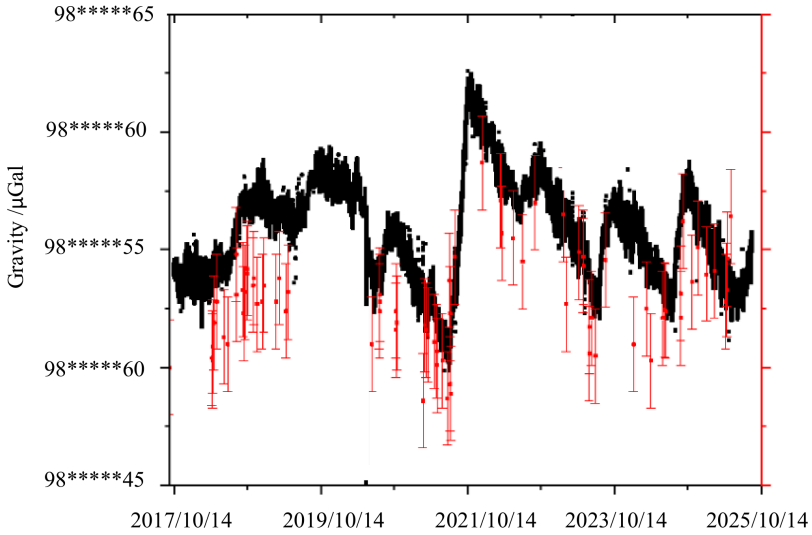

Figure 3. Gravity at the comparison sites after correction. (The red curve represents the FG5 absolute gravimeter measurements, and the black curve represents the continuous SG observations after step and drift corrections. Both datas have been corrected for solid Earth tides, polar motion, and atmospheric pressure. Asterisks indicate parts of the gravity data that are not disclosed due to confidentiality restrictions).

In 2023, FG5 participated in the international comparison, yielding a beam waist correction of 4.9 μGal and a self-gravity correction of –1.05 μGal. The comparison report listed an equivalence (Doe) of 1.94 μGal for FG5; thus, the applied correction was 1.91 μGal [24]. After removing the steps and drift from the SG data, the corrected results agreed closely with the absolute gravimeter measurements, confirming the validity of this quantitative correction method.

5.2. Drift of the SG

The estimation from the previous fitting contained errors introduced by beam waist inaccuracies and inconsistent optical alignment. For accurate long-term monitoring, a more reliable drift estimation is required. To improve precision, a new model was developed to recalculate the SG drift after step correction. Because the SG drift is very small, extending

the fitting period can improve its reliability [10]. To reduce uncertainties, the beam waist parameters of the absolute gravimeter were recalibrated, and the same operator was used. As shown in Figure 4, the 2017 KCRV values with SG and ten absolute gravimeter datasets (corrected for self-gravity and beam waist and adjusted using the 2023 comparison equivalence) were fitted against co-located SG observations using the following relation:

$$g_{\mathrm{SG}} - g_{\mathrm{AG}} = k_{rate} \cdot t_4 + c_4 \tag{7}$$

In Formula (7), g_{SG} is the SG observation, g_{AG} is the absolute gravimeter reading, and their initial difference is set to 0 μGal. k_{rate} is the SG drift rate, and c_4 is the fitting constant. A two-point constraint method was used to estimate the SG drift. The starting point is defined at the 2017 international comparison, where the SG value is assigned as zero, and the difference between the KCRV reference value and the FG5 measurement is also assumed to be zero (the FG5 was calibrated through the comparison with its DoE result). After this point, each SG observation indicates the cumulative gravity change (including instrumental drift) relative to the 2017 KCRV value. The ending point is defined by the FG5 measurements at the benchmark site after the 2023 international comparison. The difference between the SG observations (combined with the KCRV value) and the FG5 measurements at the ending point represents the total SG drift accumulated during this period.

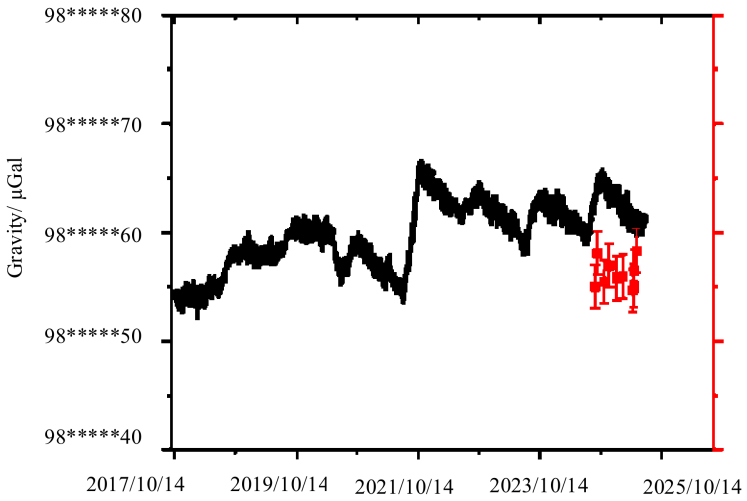

Figure 4. Gravity at the comparison sites without drift correction. The red curve represents FG5 absolute gravimeter measurements at the benchmark site after the 2023 international comparison (with accurate beam waist, self-gravity, and DoE corrections). The black points represent SG observations (after step correction but before drift removal), asterisks indicate parts of the gravity data that are not disclosed due to confidentiality restrictions.

Before 2023, FG5 measurements did not include appropriate beam waist and self-gravity corrections, resulting in systematic deviations between FG5 and SG observations. In 2023, the FG5 participated in an international comparison, from which accurate correction values were obtained. After these corrections were applied, the consistency between FG5 and SG observations improved markedly. The SG drift rate was estimated as 1.0 μGal/year, which is 0.31 μGal/year higher than the value obtained using the method described in Section 5.1. After applying the step and drift corrections, continuous gravity values at the comparison site were obtained (Figure 5).

After 2023, even after applying the correct beam waist and self-gravity corrections, small mismatches between FG5 and SG observations still remained at some points. These mismatches are mainly related to three factors: (1) the inherent uncertainty of FG5 measurements (±2 μGal); (2) the residual fitting error after step correction (6.3 μGal); and (3) gross

errors introduced during manual lighting adjustment by operators. Considering the overall measurement uncertainties, the remaining small discrepancies are considered acceptable.

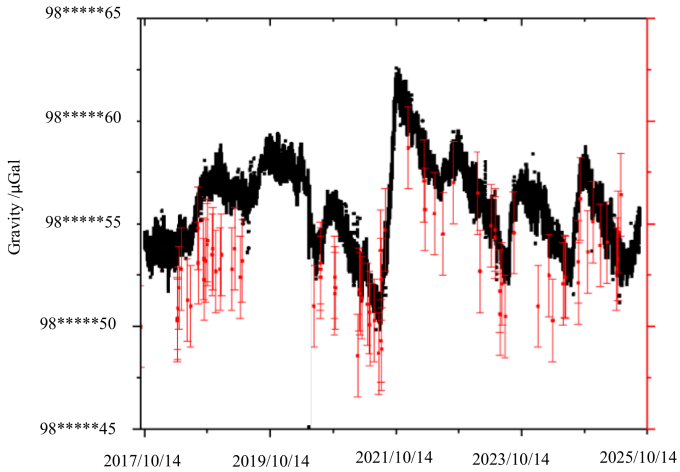

Figure 5. Gravity at the comparison sites after correction. The red dots represent FG5 absolute gravimeter measurements; the black curve represents continuous SG observations after step and drift corrections, asterisks indicate parts of the gravity data that are not disclosed due to confidentiality restrictions.

6. Analysis of the Seasonal Variations in Gravity Acceleration at the Comparison Points

6.1. Gravity and Groundwater-Level Analysis

Groundwater fluctuations can considerably affect surface gravitational acceleration [24–27]. To quantify gravity changes accurately, groundwater-induced variations near comparison sites must be removed [28]. Therefore, a survey of wells around the Changping campus of the National Institute of Metrology, China, was conducted. It was found that the China Institute of Geo-Environment Monitoring operates a water-level monitoring station (observation well) west of Sanhe Village in Nanshao town, about 7 km from the superconducting gravimeter; the well has a ground elevation of 77.695 m, a wellhead elevation of 78.195 m, and a total depth of 202 m, and monthly water-level data are recorded. Figure 6 shows observations from 1 January 2018 to 31 December 2024. In this figure, the red curve represents the processed gravity data described earlier, whereas the black curve represents groundwater-level changes. A clear correlation and phase delay can be identified between the two datasets. Considering the nonlinear relationship between gravity and groundwater, this study used correlation analysis combined with a neural network model to separate groundwater-induced gravity changes.

6.1.1. Program Design

Based on the gravity residual data and groundwater-level elevation data obtained from the previous steps, the analysis program was designed as shown in Figure 7. After initial preprocessing, the data were interpolated to synchronize the gravity acceleration and groundwater-level time series. Cross-correlation analysis was then used to determine the optimal lag step between the two datasets. Using this lag, both series were adjusted in time accordingly. After the cross-correlation step, neural network modeling and correction were carried out. The dataset was separated into training and testing subsets, with 70% of the data used for model training and 30% reserved for testing. This procedure finally produced the corrected gravity acceleration results.

The neural network architecture included one input layer (water level), one hidden layer (3–20 neurons, dynamically determined based on the training set size), and one output layer (gravity residual). The hyperbolic tangent sigmoid function (tansig) was used as the activation function in the hidden layer, and a linear function (purelin) was

applied in the output layer. The network was trained using the Levenberg–Marquardt optimizer (trainlm) with mean squared error (MSE) as the loss function and a training goal of 1×10^{-6}. The number of epochs was fixed at 1000. Early stopping with a maximum of 6 validation failures (max_fail = 6) was used to avoid overfitting. Input and output data were normalized to zero mean and unit standard deviation. The cross-correlation lag was selected by calculating the normalized cross-correlation between the normalized water level and gravity time series using the MATLAB(R2021a) xcorr function; the lag corresponding to the maximum correlation coefficient was selected. To assess model performance, the coefficient of determination (R^2), root-mean-square error (RMSE), and mean absolute error (MAE) were calculated on the test set.

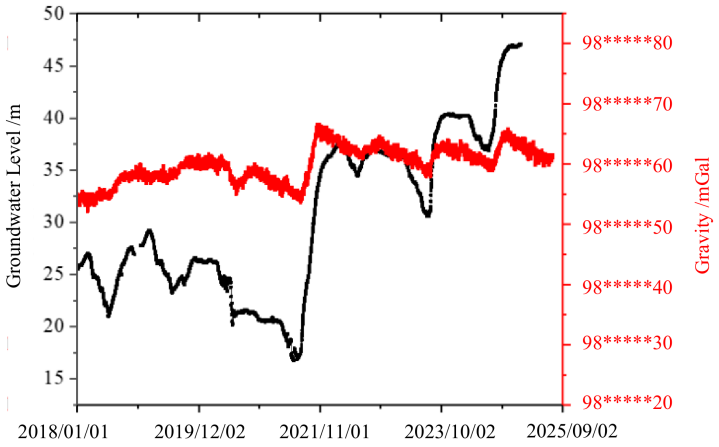

Figure 6. Gravity and groundwater level. The red line represents the variation of gravity (with corrections for solid tides, polar motion, atmospheric pressure, and drift), and the black line represents the groundwater level. Asterisks indicate parts of the gravity data that are not disclosed due to confidentiality restrictions.

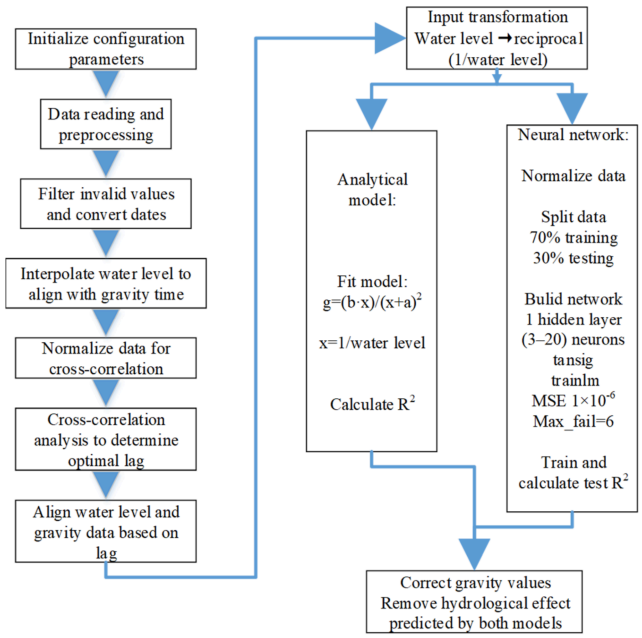

Figure 7. Program flowchart.

6.1.2. Groundwater Correction Results

After processing through the cross-correlation and neural network algorithms, the gravity acceleration before and after groundwater correction is shown in Figure 8 (left panel). The

black curve represents the uncorrected gravity acceleration, whereas the red curve indicates the data after groundwater-level correction. It is evident from the left panel that the peak-to-peak amplitude of gravity acceleration decreased from approximately 13 μGal before correction to approximately 3.5 μGal after correction. The neural network achieved an RMSE of 1.04 μGal and an MAE of 0.65 μGal on the test set. The early stopping parameter max_fail = 6 adopts the default setting of the MATLAB Neural Network Toolbox, which performed well in this study, as evidenced by the test set results (R^2 = 0.8176). This correction significantly improved data quality, effectively reducing the impact of seasonal precipitation on gravity acceleration.

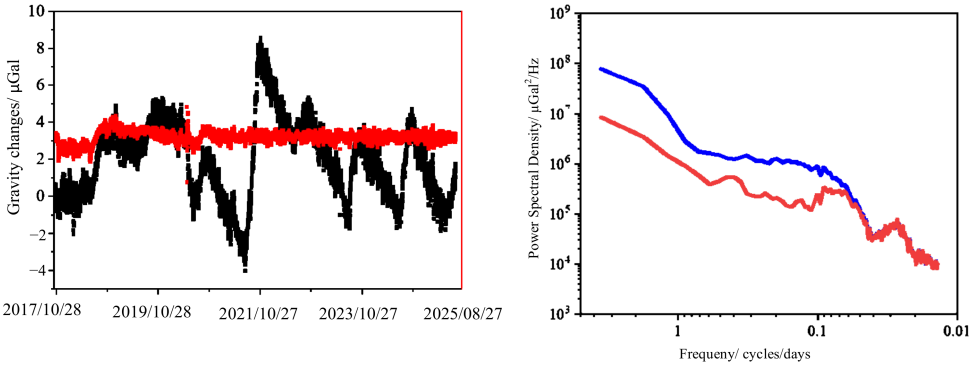

Figure 8. Gravity changes before and after groundwater correction: **Left** panel: Gravity acceleration before (black) and after (red) groundwater correction. **Right** panel: Power spectral density of gravity residuals before (blue) and after (red) neural network correction. The horizontal axis is frequency (cycles per day) on a logarithmic scale, and the vertical axis is power spectral density (μGal^2/Hz) on a logarithmic scale.

To further evaluate the effectiveness of the neural network correction, power spectral density (PSD) analysis was performed on the gravity residuals before and after correction, as shown in Figure 8 (right panel). The blue curve represents the PSD of the residuals before correction, and the red curve represents the PSD after correction. The horizontal axis is frequency (cycles per day) on a logarithmic scale, and the vertical axis is power spectral density (μGal^2/Hz) on a logarithmic scale. Before correction, the PSD exhibited significantly high energy in the long-period band (periods > 30 days, corresponding to annual and semi-annual hydrological cycles). After applying the neural network correction, the spectral energy in this long-period band was substantially reduced. The neural network reduced the long-period (>30 days) residual energy by 87.2% and the total residual energy by 81.3%, confirming its effectiveness in removing hydrological signals. In contrast, the PSD at shorter periods showed much less change, indicating that the neural network primarily removed the hydrological signal while preserving higher-frequency gravity variations. This clear spectral separation demonstrates that the neural network effectively captured and removed the local hydrological contribution from the gravity observations.

6.2. Changes in Gravitational Acceleration Caused by Ground Deformation

The surface deformation data used in this study were obtained through a customized service from the National Surface Deformation Map Service Platform of the Chinese Academy of Surveying and Mapping (CASM) (https://deformation.casm.ac.cn) (accessed on 29 November 2025), as shown in the accompanying figure. The deformation data were generated from 35 scenes of Sentinel-1 SAR images acquired from September 2023 to October 2024, using the Multi-temporal Coherent Target Small Baseline InSAR (MCTSB-InSAR) technique [29–31]. The data have a spatial resolution of 20 m and an accuracy of 4.5 mm/year, providing line-of-sight (LOS) deformation velocities and time series. Deformation data for the earlier period (2017–2022) were not available for the study site at the

time of this study, which is acknowledged as a limitation. Point 14 in Figure 9 corresponds to the reference point location. The overall deformation rate ranged from (–7~–5) mm/year. The simplified infinite-layer model (Bouguer plate model) was used to calculate the local gravity effect caused by surface deformation, as shown in Equation (8).

$$\Delta g = 2 \times \pi \times G \times \rho_{soil} \times \Delta h \quad (8)$$

G represents the gravitational constant, Δh denotes the vertical height changes (unit: m), and since the Changping area of Beijing is predominantly covered by brown loam soil, the soil density (ρ_{soil}) is 2600 kg/m^3. The resulting gravity change induced by ground deformation was approximately (0.5~0.8) μGal/year [31–33]. This variation is much smaller than that caused by groundwater fluctuations, indicating that changes in gravitational acceleration at the reference point are governed primarily by groundwater-level variations.

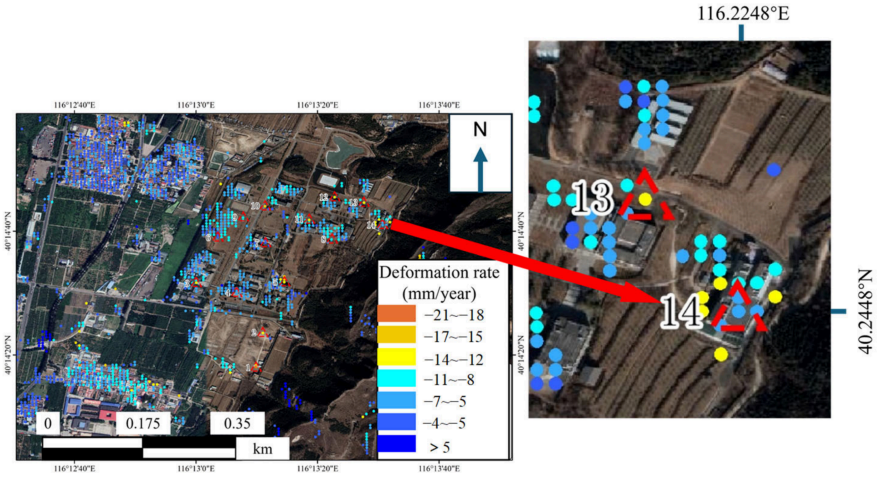

Figure 9. Ground deformation near the comparison sites. The overall deformation map of the study area (**left**) and an enlarged view (×25) around Point 14 (the benchmark site) (**right**). Point 14 is located at 116.2248°E, 40.2448°N with an elevation of 111.51 m.

7. Results

The superconducting gravimeter installed at the comparison site operated stably, indicating that the measurement consistency of the SG remained high throughout the calibration period. By joint fitting with the absolute gravimeter FG5, the step discontinuities of the SG were quantitatively corrected. The SG drift was determined to be 1.0 μGal/year. After correcting for both the steps and the drift, the SG observations were in good agreement with the absolute gravity measurements of the FG5. The main numerical results are summarized in Table 2.

Table 2. Summary of key calibration and correction results.

Parameter	Value	Uncertainty/Precision
Scale factor (weighted average)	–92.8702 μGal/V	±0.268 μGal/V (k = 1)
SG drift rate	1.0 μGal/year	±0.3 μGal/year (k = 1)
Step amplitude (2020)	31.2 μGal	1.81 μGal (standard deviation)
Step amplitude (2023)	15.2 μGal	3.21 μGal (standard deviation)
Residual fitting error (step correction)	6.3 μGal	/
Peak-to-peak (before correction)	13 μGal	/
Peak-to-peak (after correction)	3.5 μGal	/
Neural network RMSE (test set)	1.04 μGal	/
Neural network MAE (test set)	0.65 μGal	/

After applying instrumental corrections, significant seasonal variations remained in the SG residuals. Comparative analysis revealed that water-level changes around the comparison site were the dominant factor driving seasonal gravity variations. Using a neural network with local in situ water-level measurements, the peak-to-peak amplitude of gravity residuals was reduced from approximately 13 μGal to approximately 3.5 μGal.

8. Discussion

The results indicate that the scale factor shows small but measurable inter-annual variation over multi-year timescales. Therefore, assuming a constant scale factor may introduce systematic errors. It is recommended that the SG be calibrated at regular intervals and that the scale factor be considered as a time-varying parameter during data processing. The joint treatment of steps and drift is also required to maintain the continuity and accuracy of long-term gravity records. After groundwater correction using the neural network, the residual amplitude decreased to approximately 3.5 μGal, which is acceptable for the intended benchmark stability requirements, as it is comparable to the inherent uncertainty of the FG5 absolute gravimeter and much lower than the observed seasonal variation. Maintaining the long-term stability of a gravity benchmark, therefore, requires not only high-precision instrumental calibration but also co-located hydrological monitoring and targeted correction. Ignoring local hydrological processes may result in misinterpretation of actual changes in the benchmark.

The neural network combined with correlation analysis used in this study performs better than traditional forward modeling in separating hydrological gravity signals and is especially suitable for local-scale studies where reanalysis products (e.g., MERRA-2) have insufficient spatial resolution. The proposed data processing workflow is reproducible and can be directly used in other gravity monitoring networks.

9. Limitations

Several limitations of this study should be noted. First, the groundwater-level data were obtained from an observation well located approximately 7 km from the SG site. Ideally, co-located water-level measurements at the exact benchmark site would give a more accurate representation of local hydrological effects. Second, the groundwater data have a monthly temporal resolution, which may not sufficiently capture short-term hydrological fluctuations that could influence gravity variations.

Third, surface deformation data were available only for the period 2023–2024, whereas the study covers 2017–2024. Deformation data for the earlier period (2017–2022) were unavailable, which restricts the evaluation of long-term deformation effects. Fourth, this study was carried out at a single gravity comparison site. The proposed methods and findings are based on the specific conditions of this site, and their applicability to other gravity benchmark sites may differ according to local hydrological and geological conditions.

Fifth, a detailed geophysical inversion of the hydrological effects was not conducted. This is because the main focus of this study is gravity benchmark stability maintenance rather than hydrological process inversion, and our team has greater experience in benchmark maintenance and use than in geophysical inversion. This is recognized as a limitation, and collaboration with or guidance from specialists in the field is expected to support more detailed inversion studies in the future.

Sixth, we acknowledge that comprehensive uncertainty budgets (e.g., confidence intervals, statistical comparisons) were not fully established for all derived parameters. This is an aspect that we hope to improve in our future work. Greater efforts will be made to propagate uncertainties from absolute gravimeter measurements, fitting procedures, and

neural network predictions, and detailed geophysical inversion will also be conducted to better understand the underlying physical mechanisms.

Seventh, the neural network was trained using random splitting without preserving temporal order. It should be noted that random splitting may lead to information leakage and potential overestimation of model performance, whereas a chronological split would be more rigorous for time-series data. Future studies will examine time-series-aware splitting strategies to further enhance the reliability of the model.

Regarding the generalizability of the proposed workflow, although the methods are reproducible and can be adapted to other sites, the specific results remain site-dependent. Future work at multiple sites with different hydrological and geological settings is needed to further verify the broader applicability of the proposed workflow.

10. Conclusions

This study systematically assessed the stability of a gravity comparison site from 2017 to 2024. The superconducting gravimeter operated steadily throughout the seven-year period, and high-precision calibration parameters (scale factor, step corrections, and drift rate) were obtained. A segment-wise fitting method was developed to quantitatively correct step discontinuities caused by helium leakage, thereby addressing the limitations of manual Tsoft processing.

Seasonal gravity variations were found to be controlled mainly by hydrological changes rather than surface deformation. A neural network based on local in situ water-level measurements effectively removed the hydrological contribution from gravity residuals, markedly reducing the peak-to-peak amplitude. Power spectral density analysis confirmed that the neural network greatly reduced long-period residual energy. These findings provide a reference for improving SG calibration protocols, evaluating gravity benchmark stability, and developing environmental correction strategies at sites with similar hydrological and geological conditions. Further validation at multiple sites is required to confirm the broader applicability of the proposed workflow.

Author Contributions: Conceptualization, L.M.; Methodology, J.Y. and J.F.; Software, D.W., L.M. and X.C.; Validation, D.W. and X.C.; Formal analysis, Q.W.; Investigation, J.F., Q.W. and H.M.; Resources, D.W., Q.W., X.C. and M.Z.; Data curation, L.M. and D.W.; Writing—original draft, L.M.; Writing—review and editing, J.F., J.Y., H.M. and C.L.; Project administration, C.L. and M.Z.; Funding acquisition, C.L. and M.Z. All authors have read and agreed to the published version of the manuscript.

Funding: This work is supported by the National Key Laboratory of Metrology and Calibration (Grant No. JLJK2024001B003), the Central-to-Local Science and Technology Development Special Project in Hubei Province (Grant No. 2025CFC006), the National Precise Gravity Measurement Facility (Huazhong University of Science and Technology) (Grant PGMF-2024-Z003) and the Fundamental Research Funds for National Institute of Metrology, China (Grant No. AKYZZ2403, AKYZZ2501).

Institutional Review Board Statement: Not applicable.

Informed Consent Statement: Not applicable.

Data Availability Statement: The data presented in this study are available upon request from the corresponding author due to institutional data-sharing policies.

Acknowledgments: Thanks are due to Researcher Zhang Yonghong's team from the Chinese Academy of Surveying and Mapping and the China Institute of Geo-Environment Monitoring for providing data support. Thanks are due to Shaokai Wang for providing software support. All individuals named in this section have consented to the acknowledgement.

Conflicts of Interest: The authors declare no conflicts of interest.

References

1. Feng, J.Y.; Li, C.J.; Su, D.W.; Xu, J.; Wu, S. Development of absolute gravimeter and introduction on gravimetry metrological system. *Navig. Control* **2015**, *14*, 7. [CrossRef]
2. Wang, Q.Y.; Mou, L.S.; Feng, J.Y.; Li, C.J.; Su, D.W.; Wu, S.Q. Investigation on gPhone gravimeter-119 for gravity variations observation during the 10th International Comparison of Absolute Gravimeters (ICAG-2017). In Proceedings of the Tenth International Symposium on Precision Engineering Measurements and Instrumentation, Kunming, China, 8–10 August 2019; pp. 699–704. [CrossRef]
3. Wu, S.Q.; Feng, J.Y.; Li, C.J.; Su, D.W.; Wang, Q.Y.; Hu, R.; Mou, L.S. The results of 10th international comparison of absolute gravimeters (ICAG-2017). *J. Geod.* **2021**, *95*, 63. [CrossRef]
4. Hinderer, J.; Florsch, N.; Mäkinen, J.; Legros, H.; Faller, J.E. On the calibration of a superconducting gravimeter using absolute gravity measurements. *Geophys. J. Int.* **1991**, *106*, 491–497. [CrossRef]
5. Tamura, Y.; Sato, T.; Fukuda, Y.; Higashi, T. Scale factor calibration of a superconducting gravimeter at Esashi Station, Japan, using absolute gravity measurements. *J. Geod.* **2005**, *78*, 481–488. [CrossRef]
6. Imanishi, Y.; Higashi, T.; Fukuda, Y. Calibration of the superconducting gravimeter T011 by parallel observation with the absolute gravimeter FG5 #210—A Bayesian approach. *Geophys. J. Int.* **2002**, *151*, 867–878. [CrossRef]
7. Francis, O.; van Dam, T. Evaluation of the precision of using absolute gravimeters to calibrate superconducting gravimeters. *Metrologia* **2002**, *39*, 485–488. [CrossRef]
8. Calvo, M.; Hinderer, J.; Rosat, S.; Legros, H.; Boy, J.-P.; Ducarme, B.; Zürn, W. Time stability of spring and superconducting gravimeters through the analysis of very long gravity records. *J. Geodyn.* **2014**, *80*, 20–33. [CrossRef]
9. Crossley, D.; Calvo, M.; Rosat, S.; Hinderer, J. More thoughts on AG-SG comparisons and SG scale factor determinations. *Pure Appl. Geophys.* **2018**, *175*, 1699–1725. [CrossRef]
10. Van Camp, M.; Francis, O. Is the instrumental drift of superconducting gravimeters a linear or exponential function of time? *J. Geod.* **2007**, *81*, 337–344. [CrossRef]
11. Rosat, S.; Hinderer, J.; Boy, J.-P.; Littel, F.; Bernard, J.-D.; Boyer, D.; Mémin, A.; Rogister, Y.; Gaffet, S. A two-year analysis of the iOSG-24 superconducting gravimeter at the low noise underground laboratory (LSBB URL) of Rustrel, France: Environmental noise estimate. *J. Geodyn.* **2018**, *119*, 1–8. [CrossRef]
12. Rosat, S.; Boy, J.P.; Ferhat, G.; Hinderer, J.; Amalvict, M.; Gegout, P.; Luck, B. Analysis of a 10-year (1997–2007) record of time-varying gravity in Strasbourg using absolute and superconducting gravimeters: New results on the calibration and comparison with GPS height changes and hydrology. *J. Geodyn.* **2009**, *48*, 360–365. [CrossRef]
13. Mou, L.; Wang, D.; Feng, J.; Wang, Q.; Yao, J.; Ma, H.; Chen, X.; Li, C.; Zhang, M. Stability maintenance of gravity comparison sites (2017–2024): Environmental factors and data processing strategies. *Prepr. Available Res. Sq.* **2026**. [CrossRef]
14. Melchior, P. A new data bank for tidal gravity measurements (DB 92). *Phys. Earth Planet. Inter.* **1994**, *82*, 125–155. [CrossRef]
15. Falk, R.; Harnisch, M.; Harnisch, G.; Nowak, I.; Richter, B.; Wolf, P. Calibration of the superconducting gravimeters SG103, C023, CD029 and CD030. *J. Geod. Soc. Jpn.* **2001**, *47*, 22–27. [CrossRef]
16. Achilli, V.; Baldi, P.; Casula, G.; Errani, M.; Focardi, S.; Guerzoni, M.; Palmonari, F.; Raguní, G. A calibration system for superconducting gravimeters. *Bull. Géodésique* **1995**, *69*, 73–80. [CrossRef]
17. Wang, Q.Y.; Feng, J.Y.; Wang, S.K.; Zhuang, W.; Zhao, Y.; Mou, L.S.; Wu, S.Q. Calibration of the superconducting gravimeter based on a cold atom absolute gravimeter at NIM. *Chin. Phys. B* **2018**, *27*, 254–259. [CrossRef]
18. Antokoletz, E.D.; Gebauer, A.; Glässel, J.; Wziontek, H. Calibration of superconducting gravimeters by combination with absolute quantum gravimeters. In Proceedings of the EGU General Assembly 2025, Vienna, Austria, 27 April–2 May 2025. [CrossRef]
19. Chen, X.D.; Sun, H.P.; Zhang, W.M.; Hao, X.H. Precision analysis of determining the scale factor of a superconducting gravimeter using an absolute gravimeter. *Geod. Geodyn.* **2013**, *33*, 145–149.
20. Xu, J.Q.; Zhou, J.C.; Chen, X.D.; Sun, H.P. Long-term observations of gravity tides from a superconducting gravimeter at Wuhan. *Chin. J. Geophys.* **2014**, *57*, 3091–3102. [CrossRef]
21. Francis, O.; Niebauer, T.M.; Sasagawa, G.; Klopping, F.; Gschwind, J. Calibration of a superconducting gravimeter by comparison with an absolute gravimeter FG5 in Boulder. *Geophys. Res. Lett.* **1998**, *25*, 1075–1078. [CrossRef]
22. Jia, J.G.; Luan, W.; Shen, W.B. Performance analysis of the iGrav-007 superconducting gravimeter and detection of the ${}_{o}S_{m}$ spheroidal free oscillation mode. *Geomat. Inf. Sci. Wuhan Univ.* **2015**, *40*, 6.
23. Elsaka, B.; Francis, O.; Kusche, J. Calibration of the latest generation superconducting gravimeter iGrav-043 using the observatory superconducting gravimeter OSG-CT040 and the comparisons of their characteristics at the Walferdange Underground Laboratory for Geodynamics, Luxembourg. *Pure Appl. Geophys.* **2022**, *179*, 671–689. [CrossRef]
24. Boy, J.P.; Hinderer, J. Study of the seasonal gravity signal in superconducting gravimeter data. *J. Geodyn.* **2006**, *41*, 227–233. [CrossRef]
25. Crossley, D.; Hinderer, J.; Boy, J.P.; Pierce, D.W. Empirical orthogonal function (EOF) software. *Geophys. J. Int.* **2005**, *161*, 257–264. [CrossRef]

26. Neumeyer, J.; Barthelmes, F.; Dierks, O.; Flechtner, F.; Harnisch, M.; Harnisch, G.; Hinderer, J.; Imanishi, Y.; Kroner, C.; Meurers, B. Combination of temporal gravity variations resulting from superconducting gravimeter (SG) recordings, GRACE satellite observations and global hydrology models. *J. Geod.* **2006**, *79*, 573–585. [CrossRef]
27. Sato, T.; Boy, J.P.; Tamura, Y.; Matsumoto, K.; Asari, K.; Plag, H.-P.; Francis, O. Gravity tide and seasonal gravity variation at Ny-Ålesund, Svalbard in Arctic. *J. Geodyn.* **2006**, *41*, 234–241. [CrossRef]
28. Pálinkáš, V.; Lederer, M.; Kostelecký, J.; Šimek, J.; Mojzeš, M.; Ferianc, D.; Csapó, G. Analysis of the repeated absolute gravity measurements in the Czech Republic, Slovakia and Hungary from the period 1991–2010 considering instrumental and hydrological effects. *J. Geod.* **2013**, *87*, 29–42. [CrossRef]
29. Zhang, Y.; Wu, H.; Kang, Y. Ground subsidence over Beijing-Tianjin-Hebei region during three periods of 1992 to 2014 monitored by interferometric SAR. *Acta Geod. Cartogr. Sin.* **2016**, *45*, 9. [CrossRef]
30. Zhang, Y.; Wu, H.; Li, M.; Kang, Y.; Lu, Z. Investigating ground subsidence and the causes over the whole Jiangsu Province, China using Sentinel-1 SAR data. *Remote Sens.* **2021**, *13*, 179. [CrossRef]
31. Berrino, G.; Corrado, G.; Luongo, G.; Toro, B. Ground deformation and gravity changes accompanying the 1982 Pozzuoli uplift. *Bull. Volcanol.* **1984**, *47*, 187–200. [CrossRef]
32. Ukawa, M.; Fujita, E.; Ueda, H.; Nozaki, K. B19 Gravity change associated with ground deformation at Ogasawara Iwo-tou caldera. *Programme Abstr.—Volcanol. Soc. Jpn.* **2008**, 71. [CrossRef]
33. Wang, L.; Zhang, X.; Liu, Q.; Jiang, Y.; Zhao, Y.; Sun, Q.; Zhou, H.; Zhai, D.; Xiao, C.; Liu, Z. Analysis on Deformation Characteristics of Environmental Load at Anqiu Station. *Pure Appl. Geophys.* **2025**, *182*, 1601–1616. [CrossRef]

Disclaimer/Publisher's Note: The statements, opinions and data contained in all publications are solely those of the individual author(s) and contributor(s) and not of MDPI and/or the editor(s). MDPI and/or the editor(s) disclaim responsibility for any injury to people or property resulting from any ideas, methods, instructions or products referred to in the content.